Energy 149 (2018) 990–999

Contents lists available at ScienceDirect

Energy

journal homepage: www.elsevier.com/locate/energy

Minimising the effects of manufacturing uncertainties in MEMS Energy harvesters

H. Madinei*, H. Haddad Khodaparast, M.I. Friswell, S. Adhikari

College of Engineering, Swansea University, Bay Campus, Fabian Way, Crymlyn Burrows, Swansea, SA1 8EN, United Kingdom

ARTICLE INFO

Article history:
Received 16 August 2017
Received in revised form
8 February 2018
Accepted 10 February 2018
Available online 14 February 2018

Keywords:
Uncertainty
MEMS
Energy harvester
Piezoelectric
Nonlinear dynamics

ABSTRACT

This paper proposes the use of an electrostatic device to improve the performance of MEMS piezoelectric harvesters in the presence of manufacturing uncertainties. Different types of uncertain parameters have been considered and randomised according to their experimentally measured statistical properties. It has been demonstrated that manufacturing uncertainty in MEMS harvesters results in a lower output power. Monte Carlo Simulation is used to propagate uncertainty through the MEMS mathematical model. It has been found that the uncertainty effects can result in two sets of samples. The first set of samples are those with resonance frequency higher than nominal values and the second set includes samples with resonance frequencies lower than the nominal value. The device proposed in this paper can compensate for the effects of variability in the harvester by tuning the resonance frequency to the nominal design. This device is composed of a symmetrical arrangement of two electrodes, which decrease the resonance frequency from its nominal value. However, achieving precise symmetrical conditions in the device on a micro-scale is not feasible. Therefore, the effects of an unsymmetrical arrangement due to manufacturing variability are also investigated. The device includes two arch-shaped electrodes that can be used to increase the resonance frequency.

1. Introduction

In our environment, there are a variety of ambient energy sources such as solar, temperature, wind and vibration. Converting waste ambient energy into small amounts of electrical energy can power many useful low energy consuming Micro Electro Mechanical systems (MEMS) in different applications ranging from wireless sensor networks to medical implants [1–5]. Using vibration sources has gained more popularity due to their high availability in various environments. There are different transduction methods that can be used to convert mechanical vibrations into electrical energy. The most common types of transduction mechanisms are electrostatic, electromagnetic and piezoelectric. Electrostatic energy harvesters can convert ambient vibrations into electrical energy using a charged variable capacitor. The capacitance changes based on the mechanical vibrations. Any change in capacitance results in a charge rearrangement of the electrodes of the capacitor and, consequently, the charge flows through the electrical circuit [6]. Electromagnetic vibration-based energy harvesters usually consist of a coil, a permanent magnet and a suspension spring. According to the Faraday law of electromagnetic induction, when the coil experiences a change in the magnetic flux because of a relative motion between the magnet and the coil, electrical energy is generated [7]. In piezoelectric energy harvesters, the mechanical energy of vibrations is transformed into electrical energy by piezoelectric material. When piezoelectric material is deformed, the central molecules in the crystal become polarized and form a dipole. If the dipoles are arranged suitably, then two of the material surfaces become positively and negatively charged [8]. Due to the compatibility between piezoelectric material deposition and the MEMS fabrication process, piezoelectric convertors have been recognized as offering more benefits [9].

Generally, in vibration-based energy harvesters (VBEHs), maximum energy can be harvested when the harvester is excited at its resonance frequency. In most cases, the resonance frequency of the harvester does not match the frequency of the vibration source, and as a result the output power decreases significantly. There are two methods to increase the efficiency of the VBEHs: broadening the bandwidth, and tuning the resonance frequency of the harvester [10,11].

* Corresponding author.
E-mail address: hadi.madinei@swansea.ac.uk (H. Madinei).

https://doi.org/10.1016/j.energy.2018.02.048
0360-5442/

Nomenclature

$\widehat{\vartheta}_p$	Electromechanical coupling
F_e	Electrostatic force
$\widehat{\psi}$	Stochastic parameters
M_t	Tip mass
z_0	Amplitude of base excitation
$\widehat{\Omega}$	Frequency of base excitation
F_f	Follower force
$\widehat{c}_a$	Damping of the harvester
ϵ_0	Permittivity of free space
μ	Damping coefficient
C_p	Internal capacitance of the piezoelectric layer
R	Load resistance
$\overline{\epsilon}^s_{33}$	Permittivity component at constant strain
2α	Angular of overlap between the fingers
g_r	Radial gap between the comb fingers
g_{01}	Air gap between the micro-beam and the straight electrode
g_{02}	Air gap between the micro-beam and the straight electrode
$\overline{e}_{31}$	Equivalent piezoelectric coefficient
L_c	Length of piezoceramic layers
v_p	Voltage across each piezoceramic layer

In the last few years, many studies have focused on these methods to improve the harvested power of VBEHs. Masana and Daqaq [12] developed an electromechanical nonlinear model of an axially loaded energy harvester. They illustrated that the axial static load can be used to tune the system over a wide range of frequencies. Challa et al. [13] investigated a vibration energy harvesting device with autonomously tunable resonance frequency. They used a piezoelectric cantilever beam array with magnets attached to the free ends of cantilever beams to tune the system resonance frequency by magnetic force. Miller et al. [14] proposed a passive self-tuning beam resonator with sliding proof mass along the beam. This model enables the energy harvesting system to adjust the natural frequency of the system and thereby increase the energy harvested over time. Erturk and Inman [15] investigated broadband high-energy orbits in a bistable piezomagnetoelastic energy harvester over a range of excitation frequencies. Malaji and Ali [16] analysed broadband energy harvesting using multiple linear harvesters. They showed that the bandwidth of harvesting can be increased by using an array of coupled pendulums with mechanical grounding. In addition, they found that the bandwidth and the total harvested power saturates with the number of pendulums.

A mismatch between resonance frequency and vibration source frequency may exist either due to changes in working conditions, or excessive manufacturing tolerances and errors. In MEMS devices due to fabrication processes such as mask alignment, deposition, photolithography, etching and drying, manufacturing tolerances are generally high and in some cases, they can be higher than ±10% of nominal values [17]. Therefore, parameter uncertainty can significantly affect the performance of MEMS devices. Uncertainty analysis of MEMS devices has been studied by several authors of previous studies. Agarwal and Aluru [18] presented a framework to quantify different kinds of outputs in MEMS structures such as deformation and electrostatic pressure in these devices. Agarwal and Aluru [19] proposed a framework to include the effect of uncertain design parameters of MEMS devices. Based on this framework they investigated the effect of variations in Young's modulus, induced because of variations in the manufacturing process parameters or heterogeneous measurements, on the performance of a MEMS switch.

In this paper, an electrostatic device is proposed in order to compensate for the effect of manufacturing uncertainties on the performance of MEMS piezoelectric harvesters. In this model, the resonance frequency of the harvester is tuned using an arch electrode and two straight electrodes. Manufacturing uncertainty could potentially change the harvester's resonance frequency and consequently the deviation from its nominal value may be positive or negative. Therefore, there is a need to tune the harvester's resonance frequency to a higher (hardening) or lower (softening) frequency. By applying voltage to the aforementioned electrodes, the resonance frequency of the harvester can be adjusted through hardening and softening mechanisms. Applying DC voltage to the arch shaped electrode creates a tensile follower force which can increase the resonance frequency of the harvester linearly. Conversely, the resonance frequency of the harvester can be decreased by applying voltage to the straight electrodes, which creates a softening nonlinearity. The Galerkin method has been used to discretise the equations of motion. Only a single mode approximation was used in the simulations. This is mainly based on the assumption that the excitation frequencies are close to the system's first resonance frequency. The problem considered in this paper is non-linear due to the electrostatic forces. Furthermore, uncertainty in the model parameters is considered; therefore, this is a dynamic problem with the effects of both nonlinearities and uncertainties. Such problems have not received significant attention in the literature. In the presence of uncertainty, a semi-analytical solution such as Harmonic Balanace (HB) or Incremental Harmonic Balance (IHB) used by authors in previous papers [20,21] cannot be applied. This is because it is not feasible to perform a convergence study on the required number of truncated terms of nonlinear force for thousands of samples generated by Monte Carlo Simulation. This paper, for the first time to our knowledge, demonstrates the use of a shooting method in conjunction with Monte Carlo Simulation (MCS) to solve a nonlinear uncertain problem. The shooting method may be considered to be more efficient than a time integration method for uncertainty propagation. This paper also shows how nonlinear electrostatic forces, can be used to improve the performance of MEMS devices in the presence of manufacturing uncertainties.

2. Model description and mathematical modelling

Fig. 1 shows the proposed model in this paper. The model is an isotropic micro-beam of length L, width a, thickness h, density ρ and Young's modulus E, sandwiched with piezoceramic layers having length L_c, thickness h_0, Young's modulus E_0 and density ρ_0 throughout the micro-beam length and located between two straight-shaped electrodes and one arc-shaped electrode. As illustrated in Fig. 1, the piezoceramic layers are connected to the resistance (R) and the coordinate system is attached to the middle of the left end of the micro-beam, where x and z refer to the horizontal and vertical coordinates respectively. The free end of the micro-beam is attached to the two arc-shaped comb fingers, which subtend angle α at the base of the beam and remain parallel to the fixed arc-shaped electrode. The governing equation of transverse motion can be written as [22].

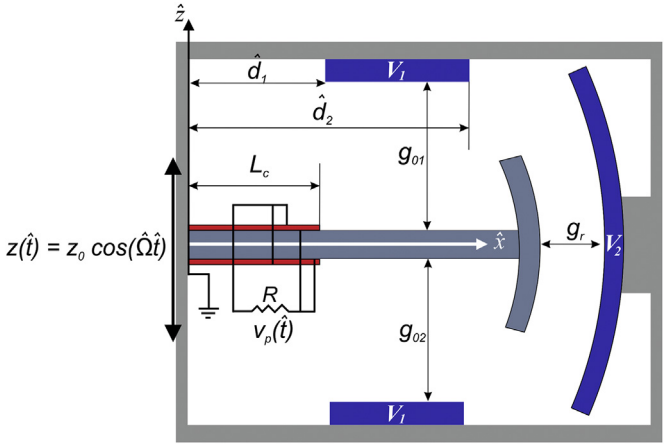

Fig. 1. Schematic of the proposed energy harvester.

$$\frac{\partial^2}{\partial\hat{x}^2}\left(EI\left(\hat{x},\hat{\psi}\right)\frac{\partial^2\hat{w}}{\partial\hat{x}^2}\right)+\rho A\left(\hat{x},\hat{\psi}\right)\frac{\partial^2\hat{w}}{\partial\hat{t}^2}+\hat{c}_a\frac{\partial\hat{w}}{\partial\hat{t}}+F_f\left(\hat{\psi}\right)\frac{\partial^2\hat{w}}{\partial\hat{x}^2}$$
$$-\hat{\vartheta}\left(\hat{\psi}\right)v\left(\hat{t}\right)\left(\frac{d\delta\left(\hat{x}\right)}{d\hat{x}}-\frac{d\delta\left(\hat{x}-L_c\right)}{d\hat{x}}\right)$$
$$=F_e\left(\hat{\psi}\right)+z_0\hat{\Omega}^2\left(\rho A\left(\hat{x},\hat{\psi}\right)+M_t\delta\left(\hat{x}-L\right)\right)\cos\left(\hat{\Omega}\hat{t}\right) \quad (1)$$

and subjected to the following boundary conditions

$$\hat{w}\left(0,\hat{t}\right)=0,\quad \frac{\partial\hat{w}\left(0,\hat{t}\right)}{\partial\hat{x}}=0$$
$$\frac{\partial}{\partial\hat{x}}\left(EI\left(\hat{x},\hat{\psi}\right)\frac{\partial^2\hat{w}\left(L,\hat{t}\right)}{\partial\hat{x}^2}\right)=M_t\left(\frac{\partial^2\hat{w}\left(L,\hat{t}\right)}{\partial\hat{t}^2}\right) \quad (2)$$
$$\frac{\partial^2\hat{w}\left(L,\hat{t}\right)}{\partial\hat{x}^2}=0$$

where $\hat{\psi}$ denotes the stochastic parameters, which have been used as an input to the mathematical model.

In Equation (1), $\hat{w}$ is the transverse deflection of the beam relative to its base at the position $\hat{x}$ and time $\hat{t}$, $\hat{c}_a$ is the viscous air damping coefficient, $\delta(\hat{x})$ is the Dirac delta function, $z(\hat{t})$ is the base excitation function, F_f is the follower force which is applied to the harvester by the arc-shaped electrode, F_e is the electrostatic force which is applied to the harvester by the straight-shaped electrodes, $v(\hat{t})$ is the voltage across the electrodes of each piezoceramic layer, $\hat{\vartheta}$ is the coupling term which is dependent on the type of connection between the piezoceramic layers (i.e. series or parallel connections). By considering the parallel connection between these layers and Kirchhoff's laws, the electrical circuit equation can be expressed by

$$C_p\left(\hat{\psi}\right)\frac{dv_p\left(\hat{t}\right)}{d\hat{t}}+\frac{v_p\left(\hat{t}\right)}{2R}+i_p\left(\hat{t},\hat{\psi}\right)=0 \quad (3)$$

where the internal capacitance (C_p), coupling term $(\hat{\vartheta}_p)$ and the current source can be obtained as [22].

$$C_p\left(\hat{\psi}\right)=\frac{\bar{\varepsilon}_{33}^S a L_c}{h_0},$$
$$\hat{\vartheta}_p\left(\hat{\psi}\right)=\frac{\bar{e}_{31}a}{h_0}\left(\left(h_0+\frac{h}{2}\right)^2-\frac{h^2}{4}\right), \quad (4)$$
$$i_p\left(\hat{t},\hat{\psi}\right)=\frac{\bar{e}_{31}a}{2}(h_0+h)\int_0^{L_c}\frac{\partial^3\hat{w}\left(\hat{x},\hat{t}\right)}{\partial\hat{x}^2\partial\hat{t}}d\hat{x}$$

In Equation (4) $\bar{e}_{31}$ is the equivalent piezoelectric coefficient and $\bar{\varepsilon}_{33}^S$ is the permittivity component at constant strain with the plane stress assumption for the beam. Using electrostatic principles, the electrostatic force between the micro-beam and the straight electrodes (F_e) can be written as [23].

$$F_e\left(\hat{\psi}\right)=\frac{\varepsilon_0 a\,H\left(\hat{x}\right)}{2}\left(\frac{V_1^2}{\left(g_{01}-\hat{w}\right)^2}-\frac{V_1^2}{\left(g_{02}+\hat{w}\right)^2}\right) \quad (5)$$

where

$$H\left(\hat{x}\right)=H\left(\hat{x}-\hat{d}_1\right)-H\left(\hat{x}-\hat{d}_2\right) \quad (6)$$

In Equation (5), ε_0 is the permittivity of free space, $H(\hat{x})$ is the Heaviside function, V_1 is the applied DC voltage to the straight electrodes, g_{01} and g_{02} are the air gaps between the micro-beam and the straight electrodes. By applying voltage to the arc-shaped electrode shown in Fig. 1, the amplitude of F_f can be tuned. Fig. 2 shows for a small angular deflection of the micro-beam (θ), the angular overlap between the fingers and the arched-shaped electrode is always 2α and the force remains a follower force in all conditions.

Based on electrostatic principles, the amplitude of the follower force (F_f) can be written as

$$F_f\left(\hat{\psi}\right)=\frac{\varepsilon_0 a}{g_r^2}V_2^2 L\alpha \quad (7)$$

where g_r is the radial gap between the comb fingers and arc-shaped electrode, a is the width of the resonator, L is the length of the beam (the thickness of the arc-shaped electrode can be ignored), and V_2 is the applied voltage to the arched-shaped electrode. For convenience, Equations (1) and (3) can be re-written in a non-dimensional form as follows

$$\frac{\partial^2}{\partial x^2}\left(s_1(x,\psi)\frac{\partial^2 w}{\partial x^2}\right)+s_2(x,\psi)\frac{\partial^2 w}{\partial t^2}+c_a\frac{\partial w}{\partial t}+\left(\alpha_f(\psi)V_2^2\right)\frac{\partial^2 w}{\partial x^2}-\vartheta_p(\psi)v_p(t)\left(\frac{d\delta(x)}{dx}-\frac{d\delta(x-l_c)}{dx}\right)$$
$$=\alpha_e(\psi)V_1^2\left(\frac{H(x)}{(1-w)^2}-\frac{H(x)}{(r(\psi)+w)^2}\right)+(\sigma_1 s_2(x,\psi)+\sigma_2\delta(x-1))\Omega^2\cos(\Omega t) \quad (8)$$

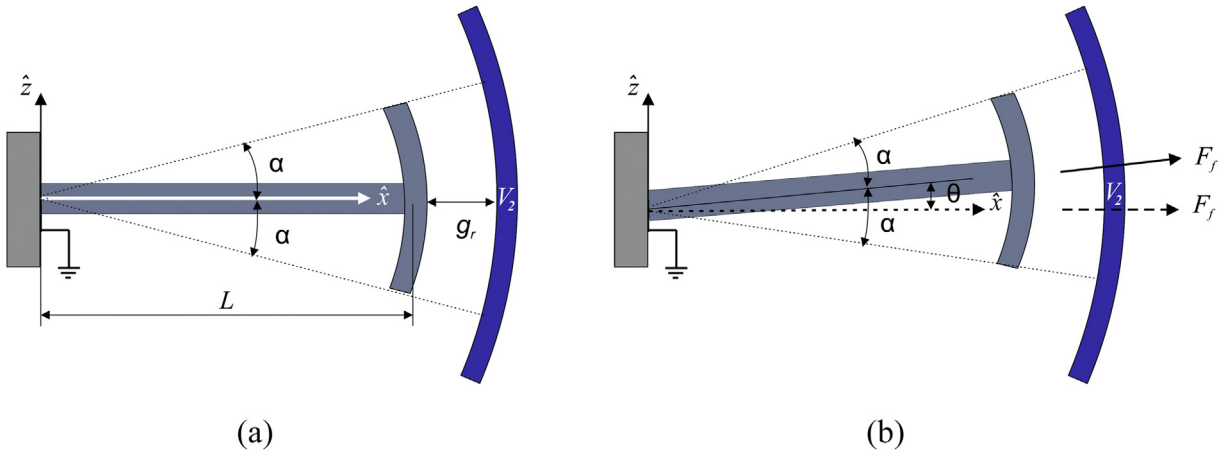

Fig. 2. A micro-beam with an arc-shaped comb fingers in its (a) unperturbed state and (b) perturbed state.

$$\frac{dv_p(t)}{dt} + \lambda(\psi)v_p(t) + \gamma(\psi)\int_0^{l_c} \frac{\partial^3 w}{\partial x^2 \partial t}dx = 0 \tag{9}$$

where

$$w = \frac{\widehat{w}}{g_{01}}, \quad x = \frac{\widehat{x}}{L}, \quad t = \frac{\widehat{t}}{T}, \quad \Omega = T\widehat{\Omega}, \quad l_c = \frac{L_c}{L}$$

$$c_a = \frac{\widehat{c}_a L^4}{(EI)_C T}, \quad T = \sqrt{\frac{(\rho A)_C L^4}{(EI)_C}}, \quad \vartheta_p = \frac{\widehat{\vartheta}_p L^2}{(EI)_C g_{01}}, \quad \alpha_f = \frac{\varepsilon_0 a L^3 \alpha}{(EI)_C g_r^2}$$

$$\alpha_e = \frac{\varepsilon_0 a L^4}{2g_{01}^3 (EI)_C}, \quad \sigma_1 = \frac{z_0 L^4 (\rho A)_C}{T^2 (EI)_C g_{01}}, \quad \sigma_2 = \frac{z_0 L^3 M_t}{T^2 (EI)_C g_{01}}, \quad \lambda = \frac{T}{2R C_p},$$

$$\gamma = \frac{\overline{e}_{31} a g_{01}(h_0 + h)}{2C_p L}, \quad r = \frac{g_{02}}{g_{01}}, \quad s_1 = \frac{EI\left(\widehat{x},\psi\right)}{(EI)_C}, \quad s_2 = \frac{\rho A\left(\widehat{x},\psi\right)}{(\rho A)_C} \tag{10}$$

where $(EI)_C$ and $(\rho A)_C$ are related to the bending stiffness and mass per unit length of the beam with piezoelectric layers. To eliminate the spatial dependence in Equations (8) and (9) the Galerkin decomposition method is used. The deflection of the micro-beam can be represented as a series expansion in terms of the eigenfunctions of the micro-beam, i.e.

$$w(x,t) = \sum_{i=1}^{N} U_i(t)\varphi_i(x) \tag{11}$$

where $\varphi_i(x)$ is the ith linear undamped mode shape of the straight micro-beam and $U_i(t)$ is the ith generalized coordinate. Equations (8) and (9) can be converted into a system of differential equations using this method. A single-mode approximation yields the following equations

$$\ddot{U}(t) + 2\mu\omega_n \dot{U}(t) + \omega_n^2 U(t) - \theta_p v_p(t) = \alpha_t \int_0^1 \left(\frac{V_1^2 H(x)}{(1 - U\varphi(x))^2} - \frac{V_1^2 H(x)}{(r + U\varphi(x))^2}\right)\varphi dx + F\Omega^2 \cos(\Omega t) \tag{12}$$

$$\dot{v}_p(t) + \lambda v_p(t) + \beta\dot{U}(t) = 0 \tag{13}$$

where

$$M = \int_0^1 s_2(x,\psi)\varphi^2(x)dx, C = c_a\int_0^1 \varphi^2(x)dx, K_f = \alpha_f V_2^2 \int_0^1 \varphi(x)\varphi^{II}(x)dx,$$

$$K_m = \int_0^1 \left(s_1^{II}(x,\psi)\varphi^{II}(x) + 2s_1^{I}(x,\psi)\varphi^{III}(x) + s_1(x,\psi)\varphi^{IV}(x)\right)\varphi(x)dx,$$

$$F = \frac{1}{M}\left(\sigma_1\int_0^1 \varphi(x)s_2(x,\psi)dx + \sigma_2\int_0^1 \varphi(x)\delta(x-1)dx\right), \quad \alpha_t = \frac{\alpha_e}{M},$$

$$\beta = \gamma\left(\frac{d\varphi(l_C)}{dx}\right), \quad \mu = \frac{C}{2M\omega_n}, \quad \omega_n = \sqrt{\frac{K_m + K_f}{M}}, \quad \theta_p = \frac{\vartheta_p}{M}\left(\frac{d\varphi(l_C)}{dx}\right) \tag{14}$$

Due to the electrostatic nonlinearity in Equation (8), finding an analytical solution to study the dynamic behavior of the system is quite complicated. However, there are different methods to find an approximate analytical solution of Equations (8) and (9). Previously, the authors (Madinei et al. [20]) have used the harmonic balance method to study the dynamic behavior of the system by considering an approximate electrostatic force using a Taylor expansion. They assumed a symmetric electrostatic force in their approximation and showed that acceptable convergence can be obtained by including terms up to ninth-order. However, in the presence of manufacturing uncertainties, the electrostatic force could be unsymmetric due to the variabilities in the air gap, and more terms may need to be included to reach acceptable convergence. Therefore, using the harmonic balance method makes the uncertainty propagation tedious because for every different sample, the number of truncated terms should be determined. In this study, the shooting method [24] is used to investigate the dynamic behavior of the system. Generally, the shooting method is a powerful and useful method to find periodic solutions to a nonlinear system, and it is computationally more time efficient than direct integration methods. The shooting method can also find unstable solutions although this is not needed for the analysis undertaken in this paper. By introducing $X_1 = U, X_2 = \dot{U}$ and $X_3 = v_p$, Equations (12) and (13) can be rewritten as

$$\dot{X}_1 = X_2, \tag{15}$$

$$\dot{X}_2 = F\cos(\Omega t) - 2\mu\omega_n X_2 - \omega_n^2 X_1 + \theta_p X_3 + \alpha_t V_1^2 \int_0^1 \left(\frac{H(x)}{(1-X_1\varphi(x))^2} - \frac{H(x)}{(r+X_1\varphi(x))^2} \right) \varphi \, dx \tag{16}$$

$$\dot{X}_3 = -\lambda X_3 - \beta X_2 \tag{17}$$

To find a periodic solution to Equations (15)–(17), an appropriate set of initial conditions (η_1, η_2, η_3) must be identified. To proceed with the shooting technique, for convenience, the following variables are defined:

$$\begin{aligned} &X_4 = \frac{\partial X_1}{\partial \eta_1}, X_5 = \frac{\partial X_1}{\partial \eta_2}, X_6 = \frac{\partial X_1}{\partial \eta_3}, \\ &X_7 = \frac{\partial X_2}{\partial \eta_1}, X_8 = \frac{\partial X_2}{\partial \eta_2}, X_9 = \frac{\partial X_2}{\partial \eta_3}, \\ &X_{10} = \frac{\partial X_3}{\partial \eta_1}, X_{11} = \frac{\partial X_3}{\partial \eta_2}, X_{12} = \frac{\partial X_3}{\partial \eta_3} \end{aligned} \tag{18}$$

The shooting technique requires the simultaneous integration of Equations (15)–(17) plus the time derivatives of the variables $(\dot{X}_4 - \dot{X}_{12})$ in the time domain for one period of excitation. The initial conditions for solving the set of differential equations are defined as

$$\begin{aligned} &X_1(0) = \eta_{10}, \ X_2(0) = \eta_{20}, \ X_3(0) = \eta_{30}, \ X_4(0) = 1, \\ &X_5(0) = 0, X_6(0) = 0, X_7(0) = 0, \ X_8(0) = 1, \\ &X_9(0) = 0, X_{10}(0) = 0, X_{11}(0) = 0, X_{12}(0) = 1 \end{aligned} \tag{19}$$

η_{10}, η_{20} and η_{30} are initial guesses for the initial condition that result in a periodic solution. Generally, these initial guesses deviate from the exact values by an error or correction $\delta\boldsymbol{\eta}$. By calculating the values of $X_4 - X_{12}$ at one period and substituting them in the algebraic system of equations below, the error can be found for each set of initial guesses [24].

$$\begin{bmatrix} \begin{bmatrix} X_4 & X_5 & X_6 \\ X_7 & X_8 & X_9 \\ X_{10} & X_{11} & X_{12} \end{bmatrix} - [I] \end{bmatrix} \begin{bmatrix} \delta\eta_1 \\ \delta\eta_2 \\ \delta\eta_3 \end{bmatrix} = \begin{bmatrix} \eta_{10} - X_1(T, \eta_{10}, \eta_{20}, \eta_{30}) \\ \eta_{20} - X_2(T, \eta_{10}, \eta_{20}, \eta_{30}) \\ \eta_{30} - X_3(T, \eta_{10}, \eta_{20}, \eta_{30}) \end{bmatrix} \tag{20}$$

By trying different initial guesses and using Equation (20), the error $(\delta\eta_1, \delta\eta_2$ and $\delta\eta_3)$ can be minimized and convergence is achieved. Then, the peak power through the resistance can be obtained by substituting v_p into the following equation

Table 1
Geometrical and material properties of the harvester.

Length, L (μm)	3000
Width, a (μm)	1000
Thickness, h (μm)	4
Thickness, h_0 (μm)	2
Young's modulus, E (GPa)	169.6
Young's modulus, E_0 (GPa)	65
Air gap, g_0 (μm)	40
Air gap, g_r (μm)	3
Damping coefficient, c_a(N.s/m)	0.002
Density of Si beam, ρ (kg/m^3)	2330
Density of PZT, ρ_0(kg/m^3)	7800
Equivalent piezoelectric coefficient, $\bar{e}_{31}$ (Cm^{-2})	−11.18
Permittivity component, $\bar{\varepsilon}_{33}^s$(nF/m)	13.48

Table 2
Most sensitive parameters to manufacturing uncertainties [17].

Data	Mean	Std	COV (%)
Thickness, h (μm)	4	0.35	8.75
Thickness, h_0 (μm)	2	0.175	8.75
Young's modulus, E (GPa)	169.6	16.58	9.78
Young's modulus, E_0 (GPa)	65	6.35	9.78
Air gap, g_0 (μm)	40	2.52	6.3
Air gap, g_r (μm)	3	0.18	6.3

$$P_0 = \frac{v_p^2}{R} \tag{21}$$

3. Numerical results and discussion

To demonstrate the analysis presented in the previous section, a bimorph piezoelectric micro cantilever beam is considered with the geometrical and material properties as listed in Table 1.

Based on the experimental results [17], the most important variations in the fabrication parameters include thickness, air gap and Young's modulus. To show the effect of these parameters on the performance of the harvester, a Gaussian distribution of parameters is assumed and given in Table 2. There are generally two models that can be used to represent parametric uncertainties, that may be categorized into two groups: (i) probabilistic and (ii) non-probabilistic. There are several models within these two categories for modelling uncertainty in numerical models. Details of these models and methods of uncertainty propagation through numerical model can be found in Refs. [25,26]. However, these are not the concern of this paper.

Considering the mean parameters of the micro-beam, the optimal resistance of the harvester is obtained at its resonance frequency. As shown in Fig. 3a, by exciting the harvester at its resonance frequency, 12.6 nW power can be harvested at the optimal resistance. In addition, as Fig. 3b shows, the maximum deflection of the beam at the resonance frequency is less than 40μm. To investigate the effect of the manufacturing uncertainties on the performance of the MEMS piezoelectric harvester, different numbers of samples are generated, and the Monte Carlo simulation is used for uncertainty propagation. Fig. 4a shows that the Probability Density Function (PDF) of the power does not significantly change when the number of samples is increased from 1500 to 2000, hence 2000 samples will be enough for uncertainty analysis.

Due to the variability of the parameters, there is a large deviation in the resonance frequencies of the samples, and this can significantly decrease the performance of the harvester. Fig. 4b shows that the mean resonance frequency of the harvester is 406 Hz, however, there are many samples which have resonance frequencies either greater or less than the mean value. On the other hand, because of this variability in resonance frequency, the harvested power of most samples deviates from the power of the system with the mean parameters when it is excited at the mean/nominal resonance frequency (see Fig. 4a). In order to compensate for the effect of manufacturing uncertainties, the resonance frequency of samples can be adjusted by applying voltage to the electrodes. Fig. 5a shows that by applying voltage to the straight electrodes, the resonance frequency of the micro-beam decreases due to the softening nonlinearity of the electrostatic field. Considering this nonlinearity, there are multiple solutions for the micro-beam response within the frequency range close to the frequency of the vibration source. In order to harvest more power, the micro beam response should be at the higher of the two solutions and

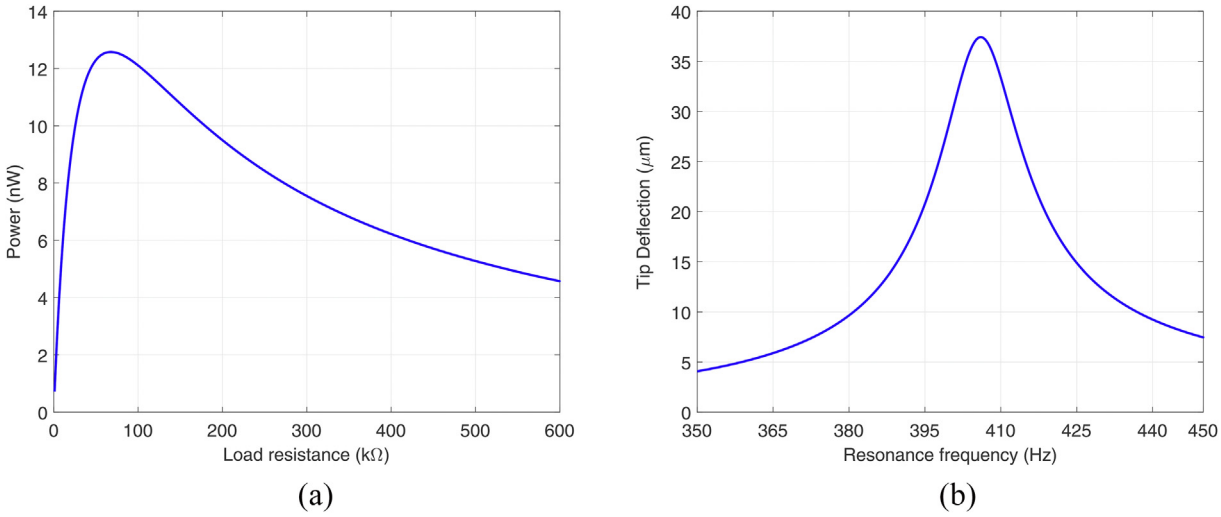

Fig. 3. (a) Variation of the piezoelectric peak power with load resistance at nominal resonance frequency (b) Displacement frequency response curve with the optimal resistance.

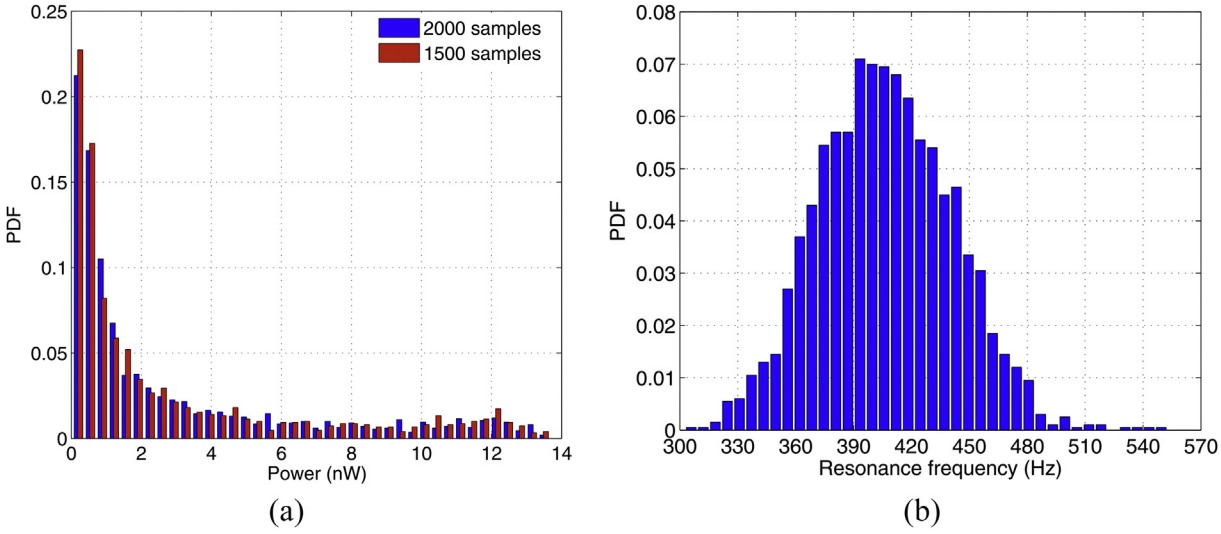

Fig. 4. Probability density function of (a) harvested power and (b) resonance frequency.

close to the resonance frequency. However, being at the higher solution depends on the initial conditions and therefore the response at the higher amplitude cannot be guaranteed. Adjusting the applied DC voltage can ensure that the response of the harvester will be in the higher solution. For a given excitation frequency if the harvester response happens to be in the lower amplitude solution the DC voltage is increased until a region is reached where the harvester only has a single solution. The DC voltage is then slowly reduced and the harvester follows high amplitude solution until the resonance is obtained.

As shown in Fig. 5a, by applying 8 V to the electrodes, the resonance frequency of the sample is decreased by 7.5% to match the frequency of vibration source. Consequently, the harvested power can be increased by 13.2 nW. Fig. 5b shows that the resonance frequency of the micro-beam can be increased by applying a follower force. In Fig. 5b, an arbitrary sample with a resonance frequency less than 406 Hz has been considered. Using the hardening mechanism and applying 13.6 V, the resonance frequency of the sample can be increased by 7.7% and therefore more power can be harvested.

In both mechanisms, the resonance frequency of the sample is tuned based on the electrostatic force. The magnitude of this force can be controlled by voltage, air gap and overlapping area between electrodes. Generally, the air gap and overlapping area are considered to be designed parameters and they are constant. However, based on Table 2, the air gaps between electrodes will be affected by manufacturing uncertainties. Therefore, depending on the air gaps between electrodes, the resonance frequency of a sample can be tuned by applying DC voltage. In the hardening mechanism, by applying voltage to the arch-shape electrodes, the resonance frequency of the harvester is changed linearly. However, due to the geometric configuration of the electrodes, in the softening mechanism the behavior of the harvester is affected by electrostatic nonlinearity.

In addition, due to the variabilities in the air gap between two straight electrodes the system may become unsymmetrical. According to Equation (5), the amplitude of the electrostatic force can be controlled by applying a DC voltage (V_1) and changing the air gap between electrodes. As shown in Fig. 6a, by considering equal initial gaps between electrodes $(g_{01} = g_{02} = 40\mu m)$, the resonance

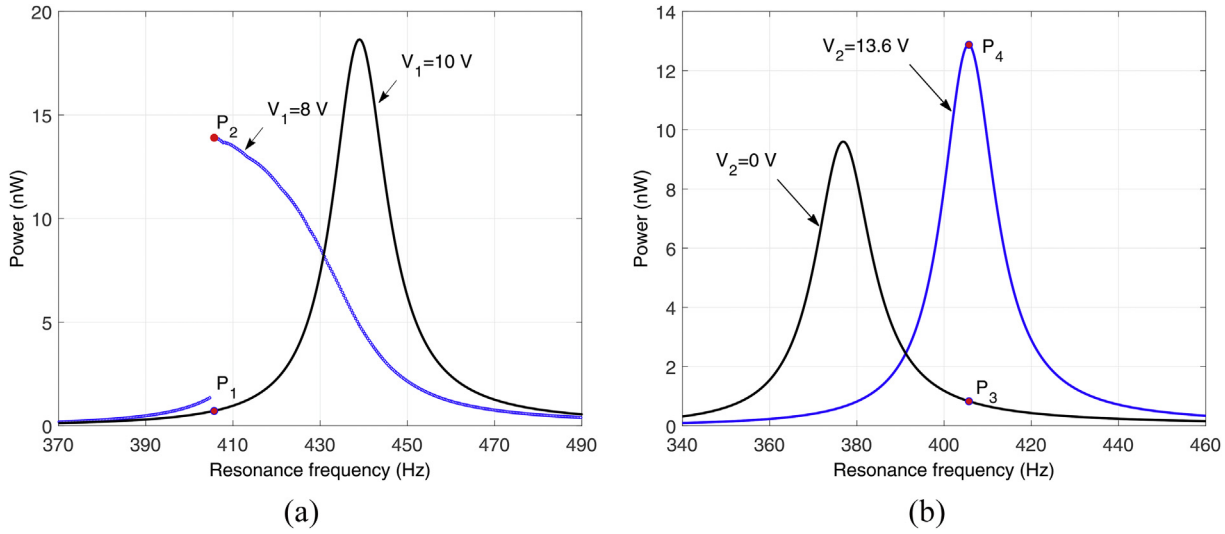

Fig. 5. Tuning resonance frequency of micro beam using (a) softening ($d_2 - d_1 = 0.5L$) and (b) hardening ($\alpha = 30^{\circ}$) mechanism.

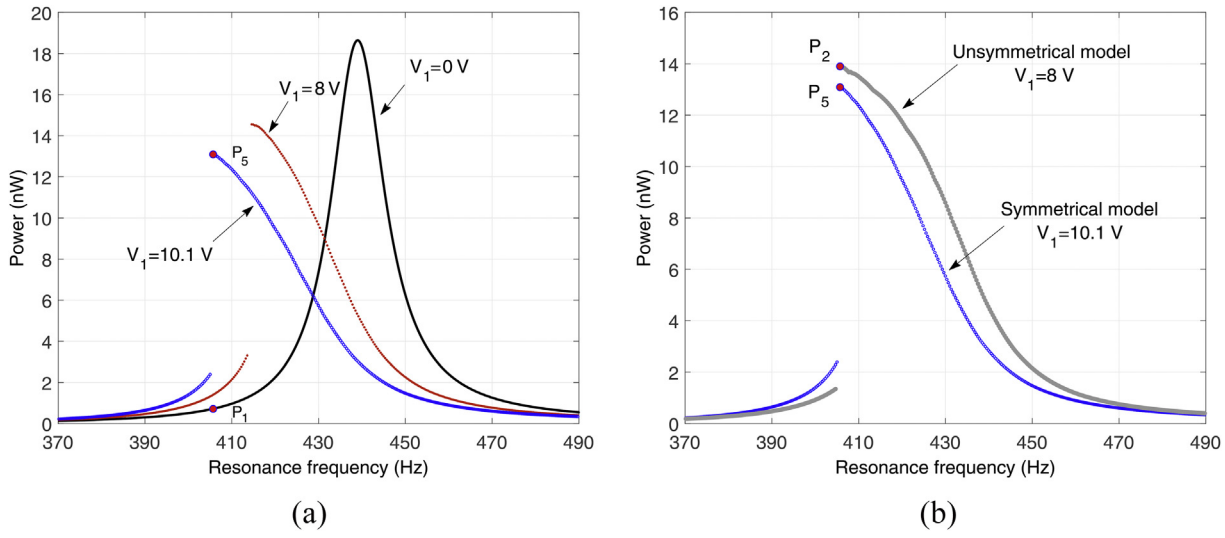

Fig. 6. (a) Tuning resonance frequency of symmetrical model ($g_{01} = g_{02} = 40\mu m$) (b) comparison of symmetrical and unsymmetrical model ($g_{01} = 44.6\mu m, g_{02} = 36\mu m$).

frequency of the sample can be tuned to the nominal frequency by applying 10.1 V to the electrodes. However, by including the variabilities in the air gaps, the resonance frequency for the given sample may be changed by applying 8 V to the electrodes (See Fig. 6b). Therefore, in comparison with the symmetrical model, depending on the initial gaps between electrodes in the unsymmetrical model, the applied DC voltage may either be increased or decreased. In addition, as shown in Fig. 7, the output power due to the steady state response for the unsymmetrical model can be different in comparison with the symmetrical model. In the unsymmetrical model, due to the nonzero static deflection, the output voltage will be affected by a DC offset. Therefore, the output voltage will swing between two different values, instead of the usual $+v_{ac}$ and $-v_{ac}$. Consequently, there will be double peaks in the steady state response of the output power in the unsymmetrical model (see Fig. 7a).

Generally, in nonlinear energy harvesters, maximum power can be harvested when the harvester responds on the upper branch in the vicinity of its resonance frequency. For any changes in the initial condition, the harvester tends to jump down to the lower branch, thereby decreasing harvested power significantly. As shown in Fig. 8a, by jumping down from point P_2 in Fig. 6b the harvested power decreases by 89%.

Fig. 8b shows that in the case of jumping down to the lower solution (P_0), the applied DC voltage is increased until a region is reached where the harvester only has a single solution. Then by delivering a gradually decreasing voltage in the fixed frequency direction, the harvester follows the high amplitude solution until resonance is obtained.

The voltage source in both symmetrical and unsymmetrical models can be charged through the harvested power from the electrostatic side. Generally, electrostatic harvesters require an energy cycle to convert mechanical energy to electrical energy [27]. The energy conversion cycles mostly rely on charge or voltage constraint concepts. In both cycles, electrical charge is stored in a variable capacitor when its capacitance is high. Then the capacitance of the capacitor is reduced by mechanical vibration, and eventually the capacitor will be discharged.

Considering the voltage constraint cycle, as shown in Fig. 9a, there are two variable capacitors between the beam and the

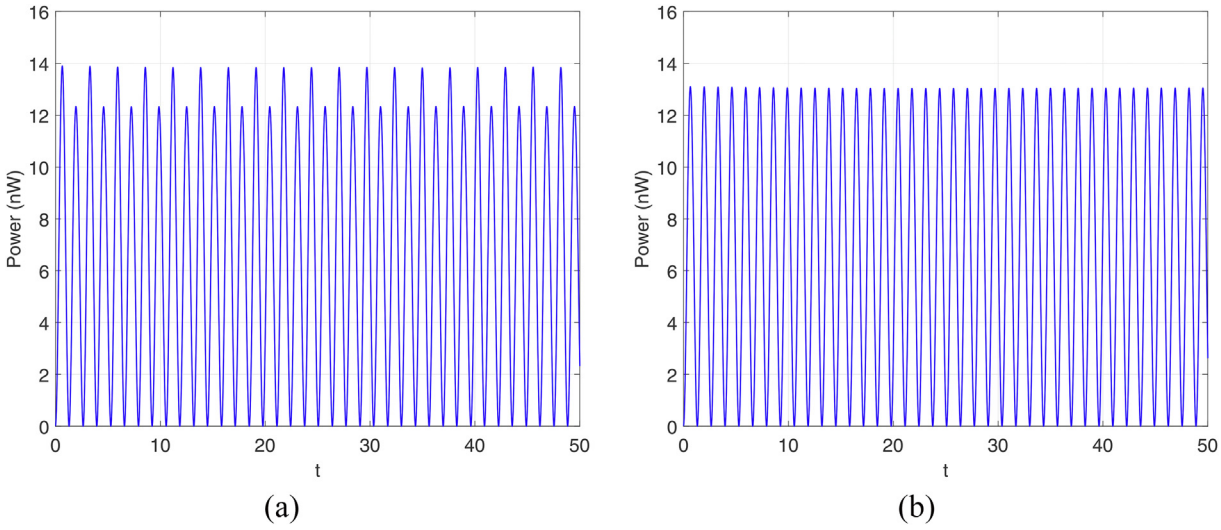

Fig. 7. Output power due to the steady state response at 406 Hz (a) unsymmetrical model ($V_1 = 8V$) (b) symmetrical($V_1 = 10.1V$).

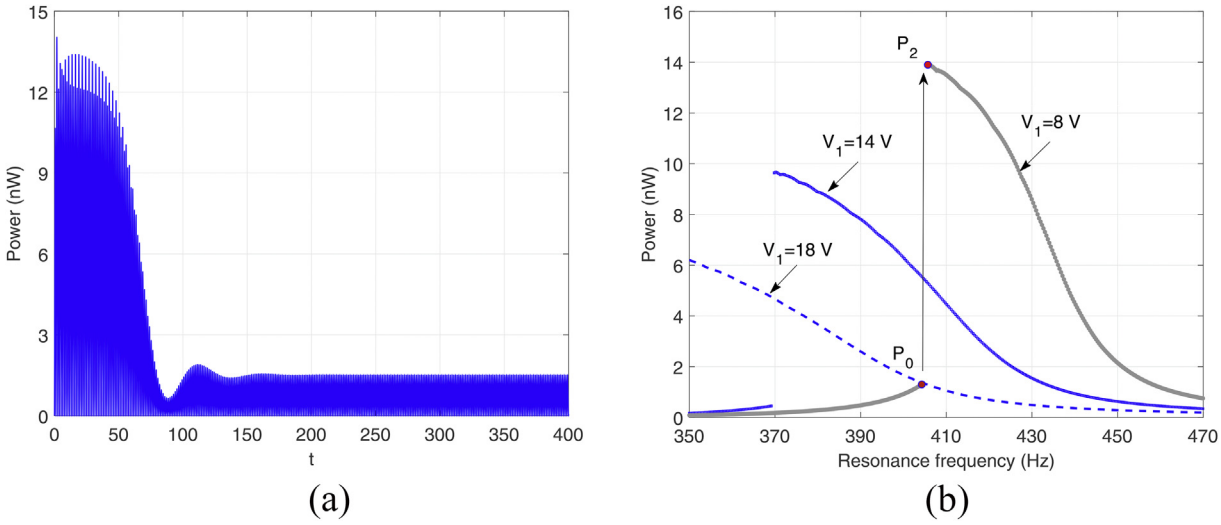

Fig. 8. (a) The output power of the harvester on the lower branch ($\Omega = 406\,Hz, V_1 = 8\,V$) (b) Moving from the lower branch to the higher one by decreasing the voltage.

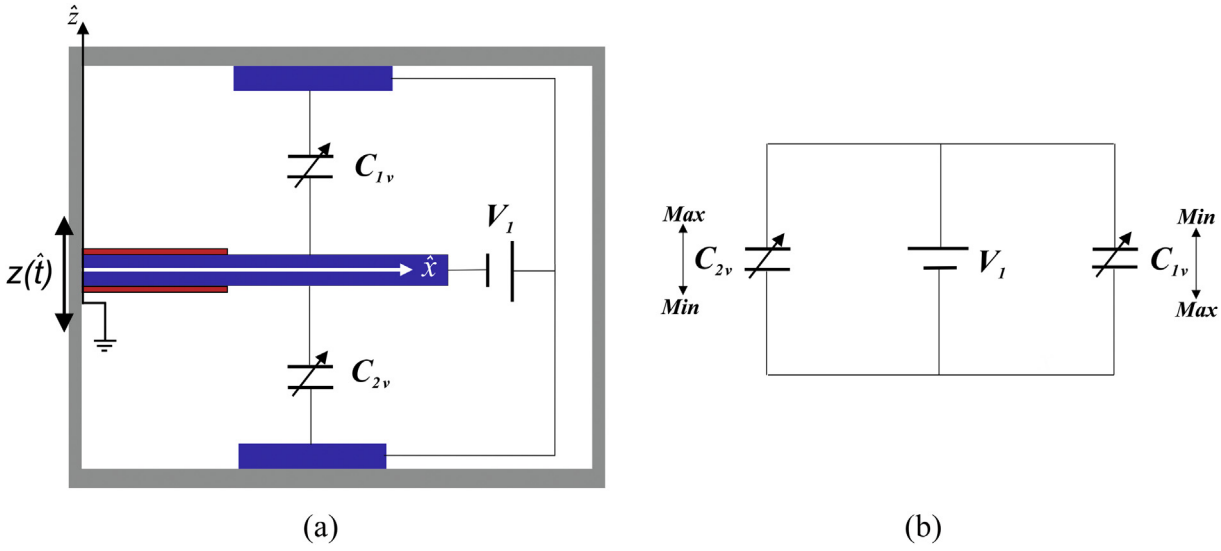

Fig. 9. (a) Variable capacitors in the proposed model (b) Electrical circuit.

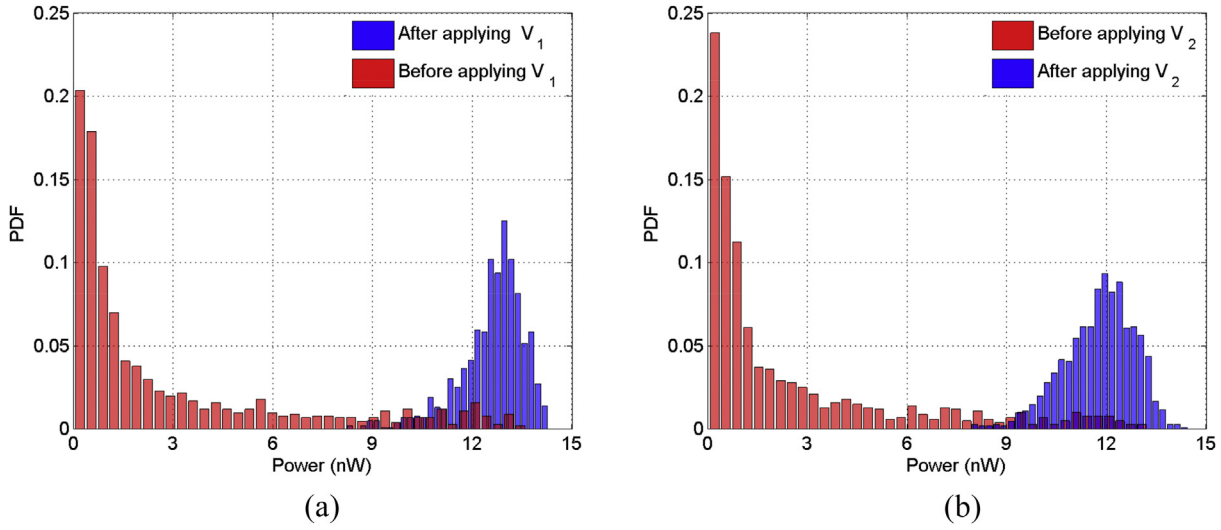

Fig. 10. Harvested power of samples based on (a) softening and (b) hardening mechanism.

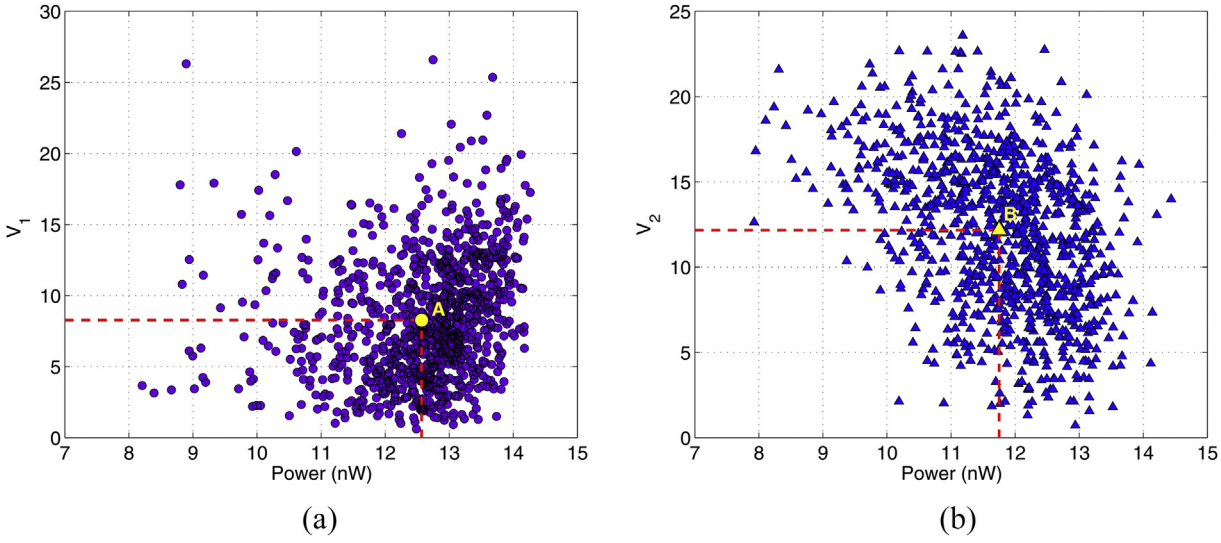

Fig. 11. (a) Applied DC voltage versus harvested power for softening mechanism and (b) hardening mechanism.

straight electrodes. In each cycle of vibration, these capacitors are charged and discharged continuously and they can charge the voltage source (V_1) based on the voltage constraint cycle. Therefore, in both symmetrical and unsymmetrical models the voltage source is self-chargeable and the harvested power from the electrostatic side is used to keep the voltage source constant [20].

Considering all samples, as shown in Fig. 10, by applying different voltages to the electrodes the resonance frequency of the samples matches the excitation frequency and more power can be harvested. Fig. 11 shows that by applying DC voltage to the straight electrodes (V_1) up to 26.6 V and the arch-electrodes (V_2) up to 24 V, the harvested power of the samples can be improved significantly. Consequently, in comparison with Fig. 4a, most samples are shifted to the region around the power of the system with the mean parameters. As shown in Fig. 11a, the mean applied DC voltage to the straight electrodes (point A) is 8.5 V and in most cases the harvested power of the samples is close to the power of the system with the mean parameters.

However, for the hardening mechanism, the mean applied DC voltage (point B in Fig. 11b) is 12.2 V, which is 3.7 V greater than the

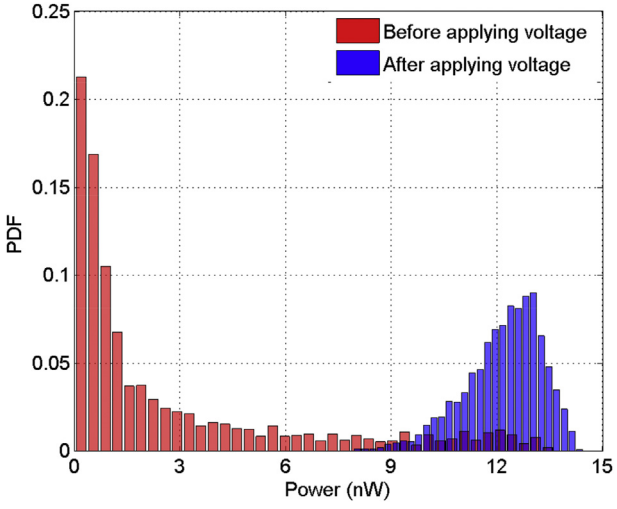

Fig. 12. Harvested power of samples before and after applying DC voltage.

mean applied DC voltage for the softening mechanism. Furthermore, the mean harvested power of the samples for the hardening mechanism is less than 12 nW. Therefore, the electrostatic nonlinearity in the softening mechanism can make the tuning mechanism more efficient in comparison with the hardening mechanism.

In the current analysis, a constant optimal resistance (70 kΩ) is used for all samples; however this resistance can be optimized for each sample [20]. In addition, since the axial deflection of the beam is negligible, the power loss of voltage source V_2 is small. Considering the results of both mechanisms, as shown in Fig. 12 by using the electrostatic force in both mechanisms, the effect of manufacturing uncertainties can be compensated and after tuning the resonance frequencies of the samples, the harvested power of the samples varies between 8 and 14 nW.

4. Conclusions

In this paper, the effect of manufacturing uncertainties on the performance of MEMS piezoelectric harvesters was investigated. The steady state solution was obtained by using the shooting method and 2000 samples were considered based on the Monte Carlo simulation. From this study, the following important conclusions were drawn:

- The results showed that variability in a MEMS harvester will significantly reduce its performance. This is because the resonance frequencies of the samples in most cases deviate from the excitation frequency and results in lower harvested power. It should be noted that the experimental data in the literature were used to randomise the model parameters.
- Two tuning mechanisms were proposed in this paper. They can be used to compensate for the effect of manufacturing uncertainty. For each sample depending on its resonance frequency, appropriate DC voltage was applied. Based on these mechanisms, it was observed that the harvested power can be increased by applying DC voltage to the straight electrodes and arch-shaped electrode up to 26.6 V and 24 V, respectively.

The problem in this paper is a nonlinear uncertain dynamic problem. One important challenge with these problems is the computational time required to solve them. It is found that using shooting method in conjunction with MCS is an efficient tool for solution of these types of problems. Future work will involve developing more efficient methods to solve this type of nonlinear uncertain problem, investigating the role of global sensitivity analysis on the selection of uncertain parameters, and robust design of such a system to passively minimise the adverse effects of uncertainty in the harvester.

Acknowledgements

Hamed Haddad Khodaparast acknowledge the support provided by the EPSRC EP/P01271X/1.

References

[1] Yang F, Du L, Chen W, Li J, Wang Y, Wang D. Hybrid energy harvesting for condition monitoring sensors in power grids. Energy 2017;118:435–45.
[2] Azizi S, Ghodsi A, Jafari H, Ghazavi MR. A conceptual study on the dynamics of a piezoelectric MEMS (Micro Electro Mechanical System) energy harvester. Energy 2016;96:495–506.
[3] Wu S, Luk PCK, Li C, Zhao X, Jiao Z, Shang Y. An electromagnetic wearable 3-DoF resonance human body motion energy harvester using ferrofluid as a lubricant. Appl Energy 2017;197:364–74.
[4] Madinei H, Khodaparast HH, Adhikari S, Friswell MI, Fazeli M. Adaptive tuned piezoelectric MEMS vibration energy harvester using an electrostatic device. Eur Phys J Spec Top 2015;224(14):2703–17.
[5] Madinei H, Keyvani-Janbahan A-A, Atashparva M, Shabani R, Rezazadeh G. Modeling of a bio sensor based on detection of antigens concentration using an electrically actuated micro cantilever. Sensor. Transduc. 2011;125(2):238.
[6] Farid Ullah K, Muhammad Usman Q. State-of-the-art in vibration-based electrostatic energy harvesting. J Micromech Microeng 2016;26(10), 103001.
[7] Rajarathinam M, Ali SF. Energy generation in a hybrid harvester under harmonic excitation. Energy Convers Manag 2018;155:10–9.
[8] Zhou Z, Qin W, Zhu P. Harvesting acoustic energy by coherence resonance of a bi-stable piezoelectric harvester. Energy 2017;126:527–34.
[9] Saadon S, Sidek O. A review of vibration-based MEMS piezoelectric energy harvesters. Energy Convers Manag 2011;52(1):500–4.
[10] Yildirim T, Ghayesh MH, Li W, Alici G. A review on performance enhancement techniques for ambient vibration energy harvesters. Renew Sustain Energy Rev 2017;71:435–49.
[11] Yildirim T, Ghayesh MH, Li W, Alici G. A nonlinearly broadband tuneable energy harvester. J Dyn Syst Meas Contr 2016;139(1):011008–11.
[12] Masana R, Daqaq MF. Electromechanical modeling and nonlinear analysis of axially loaded energy harvesters. J Vib Acoust 2010;133(1):011007–10.
[13] Vinod RC, Prasad MG, Frank TF. Towards an autonomous self-tuning vibration energy harvesting device for wireless sensor network applications. Smart Mater Struct 2011;20(2), 025004.
[14] Miller LM, Pillatsch P, Halvorsen E, Wright PK, Yeatman EM, Holmes AS. Experimental passive self-tuning behavior of a beam resonator with sliding proof mass. J Sound Vib 2013;332(26):7142–52.
[15] Erturk A, Inman DJ. Broadband piezoelectric power generation on high-energy orbits of the bistable Duffing oscillator with electromechanical coupling. J Sound Vib 2011;330(10):2339–53.
[16] Malaji PV, Ali SF. Broadband energy harvesting with mechanically coupled harvesters. Sensor Actuator Phys 2017;255:1–9.
[17] Alexeenko A, Chigullapalli S, Zeng J, Guo X, Kovacs A, Peroulis D. Uncertainty in microscale gas damping: implications on dynamics of capacitive MEMS switches. Reliab Eng Syst Saf 2011;96(9):1171–83.
[18] Agarwal N, Aluru NR. Stochastic modeling of coupled electromechanical interaction for uncertainty quantification in electrostatically actuated MEMS. Comput Meth Appl Mech Eng 2008;197(43):3456–71.
[19] Agarwal N, Aluru NR. A data-driven stochastic collocation approach for uncertainty quantification in MEMS. Int J Numer Meth Eng 2010;83(5):575–97.
[20] Madinei H, Khodaparast HH, Adhikari S, Friswell MI. Design of MEMS piezoelectric harvesters with electrostatically adjustable resonance frequency. Mech Syst Signal Process 2016;81:360–74.
[21] Khodaparast HH, Madinei H, Friswell MI, Adhikari S, Coggon S, Cooper JE. An extended harmonic balance method based on incremental nonlinear control parameters. Mech Syst Signal Process 2017;85:716–29.
[22] Erturk A, Inman DJ. Piezoelectric energy harvesting. John Wiley & Sons; 2011.
[23] Madinei H, Rezazadeh G, Azizi S. Stability and bifurcation analysis of an asymmetrically electrostatically actuated microbeam. J Comput Nonlinear Dynam 2015;10(2):021002–8.
[24] Mohammad I. MEMS linear and nonlinear statics and dynamics. New York: Springer; 2011.
[25] Govers Y, Haddad Khodaparast H, Link M, Mottershead JE. A comparison of two stochastic model updating methods using the DLR AIRMOD test structure. Mech Syst Signal Process 2015;52–53:105–14.
[26] Khodaparast HH. Stochastic finite element model updating and its application in aeroelasticity. University of Liverpool; 2010.
[27] Blokhina E, Galayko D. Towards autonomous microscale systems: progress in electrostatic kinetic energy harvesting. In: Conference towards autonomous microscale systems: progress in electrostatic kinetic energy harvesting; 2016. p. 744–7.